

# Europa's Differentiated Internal Structure: Inferences from Four Galileo Encounters

J. D. Anderson, G. Schubert, R. A. Jacobson, E. L. Lau,  
W. B. Moore, W. L. Sjogren

Radio Doppler data from four encounters of the Galileo spacecraft with the jovian moon Europa have been used to refine models of Europa's interior. Europa is most likely differentiated into a metallic core surrounded by a rock mantle and a water ice-liquid outer shell, but the data cannot eliminate the possibility of a uniform mixture of dense silicate and metal beneath the water ice-liquid shell. The size of a metallic core is uncertain because of its unknown composition, but it could be as large as about 50 percent of Europa's radius. The thickness of Europa's outer shell of water ice-liquid must lie in the range of about 80 to 170 kilometers.

The Galileo mission has provided four Europa encounters (E4, E6, E11, and E12; Table 1) at flyby distances close enough to reveal details of the satellite's gravitational field (1). Radio Doppler data were also generated from three more encounters (E13, E14, and E15) at altitudes of 3558, 1648, and 2519 km, but they are not included. Here, we removed all model ambiguities caused by previous inconsistent results (2) to yield a new suite of interior models based on a factor of 5 improvement in Europa's second-degree gravitational coefficients.

On the basis of radio Doppler data generated by the Deep Space Network (DSN) at three 70-m stations located at Goldstone, California (DSS14), near Madrid, Spain (DSS63), and near Canberra, Australia (DSS43), and nonlinear weighted least squares (3), we have determined coefficients in the standard spherical harmonic expansion of the gravitational potential  $V$  (4) to the third degree. All other higher degree harmonics have been set to zero. Our results reveal a satellite in hydrostatic equilibrium at the  $\pm 10$ -mgal level (5); hence, we have used the theory of equilibrium figures (6) to derive interior models consistent with the data. The data are not accurate enough (7) to determine the rigidity of materials within Europa by means of the method of periodic tidal deformations (8).

The flyby geometry for E4, E6, and E11 (Table 1), where along-track and cross-track components of the Doppler shift can be detected, is the most useful for determining gravitational perturbations. For E12 the spacecraft passed directly in front of Europa. Therefore, any gravitational perturbations for

E12 are detected by the Europa-centered trajectory bending only, whereas for the other three encounters the bending and the velocity perturbation along the orbital path contribute to the measured Doppler shift. The E11 data were considered less reliable than the E12 data because there was a gap of  $\sim 14$  min in the data (starting 4 min before closest ap-

proach), an important fraction of the  $\sim 60$ -min interval when the data were sensitive to the second-degree gravitational field.

We combined the Doppler data from all four encounters (Table 1), along with ground-based astrometric data on the positions of the four Galilean satellites and optical navigational data from the Voyager and Galileo missions to Jupiter, to obtain models of Europa's interior structure. This combined solution includes adjustments to the satellite ephemerides, obtained by numerical integration of their equations of motion. The E4 data were included for purposes of improving the Europa ephemeris, but these data had a negligible effect on the determination of the gravitational coefficients (Table 1). We included the possibility of an atmospheric drag deceleration acting during E12, when the spacecraft altitude was less than one Europa radius (4). We found that the E12 encounter data could be fit equally well with and without a drag model. Furthermore, a solution for the drag deceleration as a parameter in the model yields  $0 \pm 3 \text{ mm s}^{-1}$  in integrated velocity change. The conclusion from the E12 data is that atmospheric drag is not detected, but for the adopted scale heights (240 km below 300 km altitude and 440 km above

**Table 1.** Europa encounter geometry and gravity results. The location of the spacecraft's closest approach is given in the first three rows, where longitude is measured west of the Europa-Jupiter direction and altitude is referenced to a sphere of radius  $R = 1565 \text{ km}$  (4). The SEP angle is the elongation between the sun and Jupiter. For SEP angles greater than  $90^\circ$ , the minimum amount of phase noise is introduced into the S-band (2.3 GHz) radio wave as it propagates through solar plasma (19). The next three rows give the direction cosines of the Doppler line of sight for the Europa flyby trajectory at closest approach. The cross-track component is aligned with the Europa-spacecraft direction, the along-track component is aligned with the spacecraft's Europa-centered velocity vector, and the normal component is aligned with the spacecraft's Europa-centered orbital angular momentum vector. The quality of the available radio Doppler data depends on whether the data were coherent with hydrogen maser frequency standards at the DSN complexes. Coherency is achieved only when the spacecraft radio system is locked to a signal from a DSN station by means of its S-band transponder. Otherwise, the data are referenced to the spacecraft's crystal oscillator with its relatively poor frequency stability, unknown frequency bias, and unknown frequency drift. In fitting E4 and E6 data, we included the bias and drift as parameters in the model. These two parameters are unnecessary for the coherent E11 and E12 data. Other factors, particularly the continuity of the data and the location of data gaps with respect to the closest approach time, also affect the data quality. The last four rows give the results of the data analysis (7), with each flyby analyzed independently. In accordance with equilibrium theory (6), the coefficient  $J_2$  (the negative of  $C_{20}$ ) has been constrained a priori to  $10/3$  of  $C_{22}$ . The last row represents an estimate of the axial moment of inertia normalized to  $MR^2$  from Radau-Darwin equilibrium theory (6). It is not an independent parameter of the model but is calculated from the inferred value of  $C_{22}$ . For a sphere of constant density,  $C/MR^2 = 0.4$ .

	E4	E6	E11	E12
Latitude ( $^\circ$ )	-1.7	-17.0	25.7	-8.7
Longitude ( $^\circ$ )	36.8	324.7	140.6	225.0
Altitude (km)	697	591	2048	205
SEP ( $^\circ$ )	24.6	25.2	89.0	54.6
Direction cosines for line of sight				
Cross-track	0.772	0.656	-0.744	-0.985
Along-track	0.634	0.729	0.569	0.068
Normal	-0.035	-0.194	0.350	-0.160
Coherent Doppler?	No	No	Yes	Yes
$J_2$ ( $10^{-6}$ )	$215 \pm 102$	$438 \pm 45$	$442 \pm 28$	$438 \pm 9$
$C_{22}$ ( $10^{-6}$ )	$65 \pm 31$	$132 \pm 13$	$133 \pm 8$	$132 \pm 2$
$\mu$	0.999	0.995	0.986	0.847
$C/MR^2$	$0.264 \pm 0.041$	$0.347 \pm 0.014$	$0.349 \pm 0.009$	$0.348 \pm 0.002$

J. D. Anderson, R. A. Jacobson, E. L. Lau, W. L. Sjogren, Jet Propulsion Laboratory, California Institute of Technology, Pasadena, CA 91109, USA. G. Schubert and W. B. Moore, Department of Earth and Space Sciences, Institute of Geophysics and Planetary Physics, University of California, Los Angeles, CA 90095, USA.

300 km altitude), there is a  $1\sigma$  upper limit on surface atmospheric density of  $3 \times 10^{-11} \text{ kg m}^{-3}$ . This limit is consistent with radio occultation results (9).

Because the given orientation of the satellite's axes predates the Voyager mission, we included all five second-degree gravitational coefficients in the fit to the combined data. The two first-order harmonics  $C_{21}$  and  $S_{21}$  can be interpreted as corrections to the orientation of the polar axis, whereas the coefficient  $S_{22}$  measures a rotation of the  $x$  and  $y$  axes about the polar axis  $z$ . By definition, the origin of coordinates is at Europa's center of mass; hence, the first-degree harmonics  $C_{10}$ ,  $C_{11}$ , and  $S_{11}$  are all zero and were not included in the fit. The seven third-degree coefficients were included in the fit, but it is the second-degree field that provides the important constraints on the interior structure, and those coefficients (in units of  $10^{-6}$ ) are  $J_2 = 435.5 \pm 8.2$ ,  $C_{21} = -1.4 \pm 6.0$ ,  $S_{21} = 14 \pm 12$ ,  $C_{22} = 131.0 \pm 2.5$ ,  $S_{22} = -11.9 \pm 2.9$ , and  $\mu = 0.993$  (the coefficient  $\mu$  represents the correlation between  $J_2$  and  $C_{22}$  from the post-fit covariance matrix).

The lack of a definite detection of  $C_{21}$  and  $S_{21}$  indicates that the orientation of Europa's polar axis needs no correction. If the  $x$  axis is aligned in the Europa-Jupiter direction, along the smallest principal moment of inertia  $A$ , then  $S_{22}$  should be zero. The negative value of  $S_{22}$  implies that the axis along  $A$  lies  $2.60^\circ \pm 0.63^\circ$  west of the nominal  $x$  axis (10).

The major inconsistencies between the combined fit and the separate fits to each encounter (Table 1) are the  $J_2$  and  $C_{22}$  values for E4. However, the a priori hydrostatic constraint ensures that  $J_2$  is  $10/3$  of  $C_{22}$  within the error limits; hence, we are actually concerned with only one inconsistency, the parameter  $C_{22}$ . We have published plots of the Doppler residuals (observed Doppler minus model Doppler) for E4 and E6 using the fits of Table 1 (2). A similar plot of E4 residuals from the combined fit is essentially identical to the published plot. We conclude that the  $2\sigma$  bias in the  $C_{22}$  value from E4 (Table 1) is caused by systematic errors in the earlier fit to the E4 data, most likely low-frequency systematic errors in the noncoherent Doppler data.

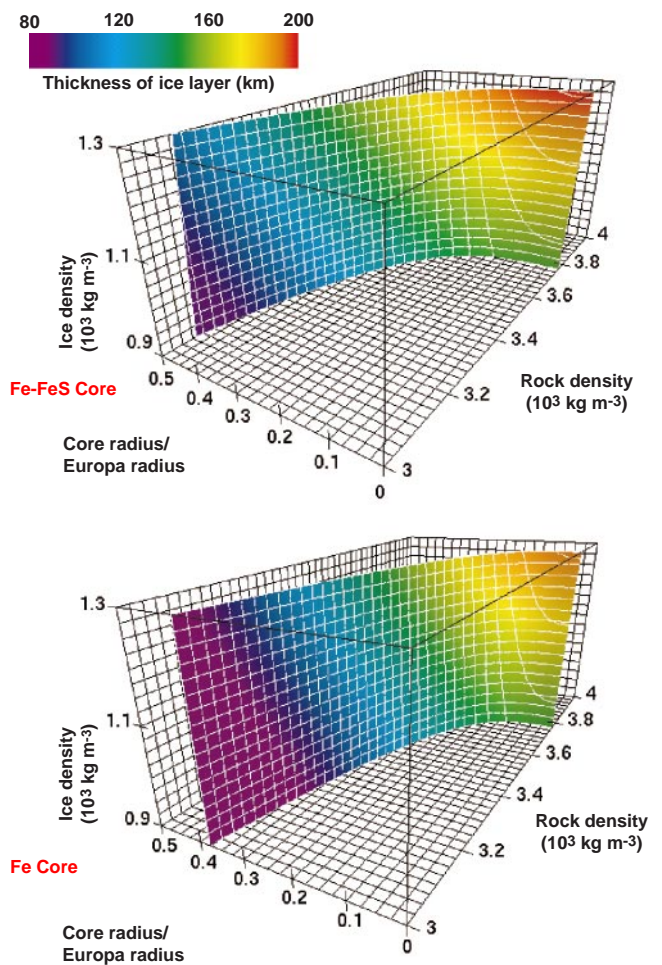
The value of  $C_{22}$  and Europa's average density (11) can be used to infer the moon's internal structure if we assume, as in our previous report (2), that the source of Europa's spherical harmonic degree 2 gravitational field is an equilibrium ellipsoidal distortion of the satellite, a distortion produced by spin and tidal forces as Europa revolves around Jupiter in synchronous rotation with its orbital period. Under these conditions,  $C_{22}$  is related to the rotational parameter  $q_r$  by

$$C_{22} = \frac{3\alpha q_r}{4} \quad (1)$$

where  $q_r$  [the ratio of the centrifugal force to the gravitational force at Europa's equator (11)] is a measure of the forcing for rotational flattening of the satellite, and  $\alpha$  is a dimensionless response coefficient that depends on the distribution of density with depth inside the satellite ( $\alpha = 0.5$  for constant density). For  $C_{22} = 131.5 \pm 2.5 \times 10^{-6}$  (10),  $\alpha = 0.3493 \pm 0.0085$ , where the errors in  $C_{22}$  and  $q_r$  respectively contribute 1.9% and 1.5% to the error in  $\alpha$  (11). From equilibrium theory and the value of  $\alpha$ , it follows that Europa's axial moment of inertia  $C$ , normalized to  $MR^2$ , is  $C/MR^2 = 0.346 \pm 0.005$ . This value of  $C/MR^2$  is less than 0.4, the value of  $C/MR^2$  for a sphere of constant density, and it requires a concentration of mass toward the center of Europa (12).

The surface of Europa is covered by a layer of water ice, which may in turn overlie a liquid water ocean (13). The gravity experiment cannot distinguish between liquid water and ice because their densities are similar, but it is clear

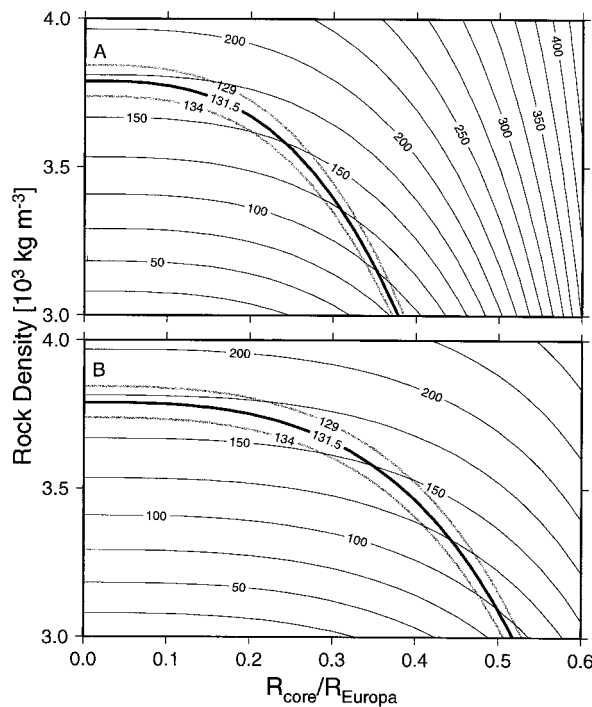
Fig. 1. Possible three-layer models of Europa consistent with its mean density and axial moment of inertia ( $C/MR^2 = 0.346$ ). Two sets of models are considered, one having Fe cores with density  $8000 \text{ kg m}^{-3}$  and the other having Fe-FeS cores with density  $5150 \text{ kg m}^{-3}$ . Any point on one of the surfaces defines an interior structure with properties given by the coordinate axis values and the color of the surface. Ice density refers to the density of the outer spherical shell of the model, which is predominantly water in either ice or liquid form with an admixture of some rock. The color of the surface gives the thickness of this outer shell according to the color bar. Rock density refers to the density of the mainly silicate intermediate shell, which may also contain some metal. Possible Europa models are defined by the surfaces whose colors give the thickness of the water ice-liquid outer shell. Other model parameters (outer shell or ice density, intermediate shell or rock density, and core radius) are provided by the coordinate axes. Two-layer Europa models are given by the intersection of the model surfaces with the core radius = 0 plane.



that the interior of Europa must have a density higher than the mean value (2). Because silicates and iron compounds are the only sufficiently abundant materials with densities in this range, we explore three-layer models consisting of a water ice or liquid outer shell, a rock layer composed of silicates or a silicate-metal mixture, and an optional metallic core composed of Fe or an Fe-FeS eutectic mixture.

Because only mean density and  $C$  constrain the models, there are too many unknowns to provide a unique inversion. We bound the parameter space with constraints on the densities of ice, including "dirty" ice-rock mixtures and some denser phases of ice that may exist near the bottom of the water ice layer, the densities of silicates and silicate-metal mixtures, the radius of the core, and the density of the core, which is either  $8000 \text{ kg m}^{-3}$  for Fe or  $5150 \text{ kg m}^{-3}$  for the Fe-FeS eutectic. We took a forward-modeling approach and solved Clairaut's equation for  $\alpha$  to determine the family of model parameters that satisfied our combined fit to all the observations. All the models have water ice-liquid shell thicknesses between  $\sim 100$  and  $200 \text{ km}$  (Fig. 1).

**Fig. 2.** Details of the intersection of the model surface of Fig. 1 with the horizontal outer shell density = 1050 kg m<sup>-3</sup> plane. Europa three-layer models having an ice density (outer shell density) of 1050 kg m<sup>-3</sup> are shown for an Fe core (A) and an Fe-FeS core (B). The solid curve labeled 131.5 (× 10<sup>-6</sup>) defines models constrained by Europa's mean density and the indicated values of C<sub>22</sub> used in constructing the model surfaces in Fig. 1. The curves designated 129 and 134 (× 10<sup>-6</sup>) delineate models with the ±1σ values of C<sub>22</sub>. The numbers within the curves denote the outer shell thickness (in kilometers).



Although two-layer models can be found that are consistent with the observations, we find these models implausible. Previously we argued for a metallic core on the basis of magnetic field perturbations observed during the E4 flyby (14). Subsequent observations have not confirmed an intrinsic European magnetic field, and are instead more consistent with plasma surrounding Europa and a time-varying induced magnetic field with a source near the surface (15). Although an intrinsic magnetic dipole would have provided powerful evidence for a metallic core, other lines of evidence allow us to use the gravity data to confirm the presence of a European core.

Models of Europa's interior that lack a metallic core are only consistent with the observed value of C<sub>22</sub> if the interior is a mixture of rock and metal with a density higher than 3800 kg m<sup>-3</sup>. This density implies that Europa's interior is enriched in dense metallic phases relative to Io, which has a bulk density of 3529 kg m<sup>-3</sup> (16). If the metal is Fe, the enrichment is 12%, and the enrichment is even greater for lower density metallic phases such as magnetite. We suggest that such degrees of enrichment in dense phases are unlikely for a smaller body forming farther out in the proto-jovian nebula than Io. It is more likely that this mixture would separate into a metallic core and rock mantle, because radiogenic heating in the silicates alone would raise Europa's interior to temperatures high enough for differentiation to occur (17), and tidal heating, though difficult to quantify, is potentially an important additional source of heating in the mantle. We therefore conclude that Europa has a differentiated metallic core, and we proceed to analyze three-layer models that can satisfy the constraint on the moment of

inertia without requiring Fe enrichment in Europa relative to Io.

The three-layer models of Europa have Fe and Fe-FeS cores of varying sizes, depending on the density of the rock mantle; lower rock densities yield larger cores and thinner water ice-liquid outer shells (Figs. 1 and 2). The minimum thickness of the water ice-liquid outer shell in the three-layer models is ~80 km. Smaller outer shell thicknesses are possible only for mantle densities lower than 3000 kg m<sup>-3</sup>. Such low mantle densities are possible only if the mantle silicates are hydrated. In effect, the water in the outer shell is trading off with the water in hydrated mantle silicates. If the mantle density is sufficiently low (<3000 kg m<sup>-3</sup>), there is enough density contrast between the mantle and the metallic core to account for the relatively small moment of inertia of Europa. Otherwise, a thick water ice-liquid shell (100 to 200 km) is needed to provide the requisite density contrast between the exterior and deep interior of a differentiated Europa. Hydrated silicates break down and release their water at temperatures between 700° and 800°C at the pressures in Europa's interior (18), making it unlikely that a thick European mantle would have an average density lower than 3000 kg m<sup>-3</sup>. Furthermore, it is implausible that Europa would have differentiated a metallic core while retaining a hydrated silicate mantle.

**References and Notes**

1. The first encounter (E4) occurred on 19 December 1996, the second (E6) on 20 February 1997, the third (E11) on 6 November 1997, and the fourth (E12) on 16 December 1997; the numerical suffixes refer to orbital revolutions of Jupiter by the spacecraft.

2. J. D. Anderson, E. L. Lau, W. L. Sjogren, G. Schubert, W. B. Moore, *Science* **276**, 1236 (1997).  
 3. See, for example, T. D. Moyer, *Tech. Rep. TR 32-1527* (Jet Propulsion Laboratory, Pasadena, CA, 1971); B. D. Tapley, in *Recent Advances in Dynamical Astronomy*, B. D. Tapley and V. Szebehely, Eds. (Reidel, Dordrecht, Netherlands, 1973), pp. 396–425; J. D. Anderson, in *Experimental Gravitation*, B. Bertotti, Ed. (Academic Press, New York, 1974), pp. 163–199.  
 4. W. M. Kaula, *Theory of Satellite Geodesy* (Blaisdell, Waltham, MA, 1966). The expression for V is

$$V(r, \phi, \lambda) = \frac{GM}{r} \left[ 1 + \sum_{n=2}^{\infty} \sum_{m=0}^n \left( \frac{R}{r} \right)^n (C_{nm} \cos m\lambda + S_{nm} \sin m\lambda) P_{nm}(\sin \phi) \right] \quad (2)$$

where M is the satellite's mass and G is the gravitational constant,  $G = 6.67259 \pm 0.00085 \times 10^{-11} \text{ m}^3 \text{ kg}^{-1} \text{ s}^{-2}$  [E. R. Cohen and B. N. Taylor, *Phys. Today* **50**, BG7 (1997)]. The spherical coordinates (r, φ, λ) are referenced to the center of mass, with r the radial distance, φ the latitude, and λ the longitude on the equator. Europa's reference radius R is 1565 ± 8 km [M. E. Davies et al., *Celest. Mech.* **53**, 377 (1992)]. P<sub>nm</sub> is the associated Legendre polynomial of degree n and order m, and C<sub>nm</sub> and S<sub>nm</sub> are the corresponding coefficients determined from the data.

5. The Galileo (gal) is a unit of acceleration (1 gal = 10<sup>-2</sup> m s<sup>-2</sup>) commonly used in gravimetry.  
 6. W. B. Hubbard and J. D. Anderson, *Icarus* **33**, 336 (1978); S. F. Dermott, *ibid.* **37**, 310 (1979); V. N. Zharkov, V. V. Leontjev, A. V. Kozenko, *ibid.* **61**, 92 (1985); S. Mueller and W. B. McKinnon, *ibid.* **76**, 437 (1988); G. Schubert, D. Limonadi, J. D. Anderson, J. K. Campbell, G. Giampieri, *ibid.* **111**, 433 (1994).  
 7. All estimated errors were taken directly from the covariance matrix associated with the data analysis. They were based on an assumed standard error of 2 mm s<sup>-1</sup> for noncoherent Doppler and 1 mm s<sup>-1</sup> for coherent Doppler at a sample interval of 60 s. For data sampled at 10 s near the closest approaches to Europa, the error was increased by √6. A weighting algorithm was applied that increased the assumed standard error on the data as the spacecraft elevation angle approached the DSN station's horizon.  
 8. An experiment to measure tidal variations on Titan during the Cassini orbital tour of the saturnian system in 2004 to 2008 has been proposed [N. Rappaport, B. Bertotti, G. Giampieri, J. D. Anderson, *Icarus* **126**, 313 (1997)]. A similar experiment for Europa is feasible, but because of the smaller eccentricity of Europa's orbit (~0.009, versus an eccentricity of 0.029 for Titan), a future Europa orbiter mission would be required.  
 9. A. J. Kliore, D. P. Hinson, F. M. Flasar, A. F. Nagy, T. E. Cravens, *Science* **277**, 355 (1997). The best estimate of the surface number density is 10<sup>14</sup> m<sup>-3</sup>, which for O<sub>2</sub> corresponds to a mass density of 5 × 10<sup>-12</sup> kg m<sup>-3</sup>, about one-sixth the value of our upper limit.  
 10. For dynamical reasons, the principal axis must be directed on average toward Jupiter. The orientation of the axes in our software [JPL's Orbit Determination program (ODP)] was defined in 1980 on the basis of Lieske's E2 ephemeris for the Galilean satellites [J. H. Lieske, *Astron. Astrophys.* **56**, 333 (1978)]. However, an adjustment of 1.54° in the location of zero longitude was made in 1982, so that Europa's 182° meridian passed through the crater Clix in accordance with IAU convention (4). Hence, the definition of zero longitude in the ODP is based on Voyager imaging data, not on satellite dynamics. If Europa followed Lieske's E2 ephemeris, the 1980 x axis would point toward Jupiter and S<sub>22</sub> would be zero. But with the 1982 definition, Jupiter would be 1.54° west of the x axis. Also, our current numerically integrated ephemeris does not agree with Lieske's E2 ephemeris, so we expect an additional offset. In the middle of November 1997 (a date between E11 and E12), the mean position of Jupiter was at west longitude 1.17°, according to our current ephemeris. The Europa gravity data yield an indirect determination for Jupiter's

cartographic longitude of  $2.60^\circ \pm 0.63^\circ$ ,  $2.3\sigma$  from the actual location given by the ephemeris. We consider this not only a satisfactory agreement, but also an excellent check on the Doppler-determined gravity. The value of  $C_{22}$  in the system of rotated axes is  $(C_{22}^2 + S_{22}^2)^{1/2}$ , and  $S_{22}$  is zero by definition. The axis rotation increases  $C_{22}$  to  $131.5 \pm 2.5 \times 10^{-6}$  and  $\mu$  is reduced from 0.993 to 0.988.

11. Our best estimate for Europa's  $GM$  is  $3202.72 \pm 0.05 \text{ km}^3 \text{ s}^{-2}$ . Using the best current values for  $G$  and  $R$  (4), we obtain a mass for Europa of  $4.79982 (\pm 0.00062) \times 10^{22} \text{ kg}$  and a mean density of  $2989 \pm 46 \text{ kg m}^{-3}$ . The rotational parameter  $q_r = \omega^2 R^3 / GM$  is  $5.019 (\pm 0.077) \times 10^{-4}$ , where the angular velocity  $\omega = 2\pi/P$  is determined from Europa's sidereal orbital period  $P = 3.551$  days [P. K. Seidelmann, *Explanatory Supplement to the Astronomical Almanac* (University Science Books, Mill Valley, CA, 1992)]. The errors in the density and  $q_r$  are dominated by the 8-km error in Europa's radius.
12. The gravity coefficient  $C_{22} = 131.5 \times 10^{-6}$  and the rotational parameter  $q_r = 5.019 \times 10^{-4}$  can also be

used to compute the equilibrium shape of the Roche-Darwin ellipsoid (6). In terms of the principal axes ( $c < b < a$ ), where  $a$  is the equatorial radius,  $c$  is the polar radius, and  $b$  is the intermediate radius, the polar flattening is  $(a - c)/c = 2.056 \times 10^{-3}$ . The distortion of the equatorial cross section can be expressed by the parameter  $(b - c)/(a - c)$ , which according to equilibrium theory is exactly 1/4. We use the axial moment of inertia  $C$  normalized to  $MR^2$  as a constraint on the interior models. We ignore the small differences between the three principal moments ( $\sim 0.1\%$ ).

13. G. Schubert, T. Spohn, R. T. Reynolds, in *Satellites*, J. A. Burns and M. S. Matthews, Eds. (Univ. of Arizona Press, Tucson, 1986), pp. 629–688; M. H. Carr *et al.*, *Nature* **391**, 363 (1998); R. T. Pappalardo *et al.*, *ibid.*, p. 365; P. E. Geissler *et al.*, *ibid.*, p. 368; R. Sullivan *et al.*, *ibid.*, p. 371.
14. M. G. Kivelson *et al.*, *Science* **276**, 1239 (1997).
15. K. K. Khurana *et al.*, *Nature*, in press.
16. J. D. Anderson, W. L. Sjogren, G. Schubert, *Science* **272**, 709 (1996).

17. Because Europa and the moon are similar in size and density, the expected temperature in an undifferentiated European mantle—produced by radiogenic heating, subsolidus convective heat transport, and temperature-dependent mantle viscosity—can be estimated from calculations carried out for the lunar interior. Lunar calculations are reported in G. Schubert, R. E. Young, P. Cassen, *Philos. Trans. R. Soc. London Ser. A* **285**, 523 (1977). The deep mantle temperature in these lunar models is between 1500 and 1600 K.
18. P. Ulmer and V. Trommsdorff, *Science* **268**, 858 (1995).
19. R. Woo and J. W. Armstrong, *J. Geophys. Res.* **84**, 7288 (1979).
20. This work was sponsored by the Galileo Project and was performed at the Jet Propulsion Laboratory, California Institute of Technology, under contract with NASA. G.S. and W.B.M. acknowledge support by grants from NASA through the Galileo Project at JPL and the Planetary Geology and Geophysics program.

6 May 1998; accepted 4 August 1998

# Origin of Multikilometer Earth- and Mars-Crossing Asteroids: A Quantitative Simulation

Fabio Migliorini,\* Patrick Michel, Alessandro Morbidelli,†  
David Nesvorný, Vincenzo Zappalà

Orbital dynamic simulations show that many asteroids in the main asteroid belt are driven toward Mars-crossing orbits by numerous weak mean motion resonances, which slowly increase the orbital ellipticity of the asteroids. In addition, half of the Mars-crossing asteroids (MCAs) transition to Earth-crossing asteroids (ECAs) in less than 20 million years. This scenario quantitatively explains the observed number of large ECAs and MCAs.

Most ECAs and MCAs are fragments of larger main belt asteroids. According to the classic scenario (1), they were injected by the collisions that formed them into a resonance (2), which increased their eccentricities until they started to cross the terrestrial planets' orbits. The encounters with the planets then spread them all over the region where they are now observed and categorized as ECAs or MCAs (3).

Recent simulations (4) showed that the median dynamical lifetime of bodies initially placed in the 3/1 or  $\nu_6$  resonances is only 2 My (million years), because these resonances pump the eccentricity to unity, forcing most of the resonant bodies to collide with the sun. As a

consequence, in order to sustain the observed planet-crossing population in steady state, the number of bodies injected into resonance per million year would need to be about 25% of the total population. This indicates that the classic scenario cannot explain the origin of multikilometer ECAs and MCAs. In fact, 10 ECAs and 354 MCAs with diameters larger than 5 km are currently known (5) despite the fact that bodies of this size can be injected into resonance only during very energetic and rare breakup events, such as those leading to formation of asteroid families (6). Also, the classic scenario would predict a lower MCA/ECA ratio than is observed because asteroids in the 3/1 and  $\nu_6$  resonances experience such a rapid increase in their eccentricity that they quickly become ECAs or graze the sun before encounters with Mars can extract the asteroids from these resonances into MCAs.

The orbital distribution of MCAs consists of four groups—hereafter denoted by MB, MB2, HU, and PH—with values of semimajor axis  $a$  and inclination  $i$  similar to those of four populations of non-planet-crosser asteroids: the main belt below the  $\nu_6$  resonance, the main belt above the  $\nu_6$  resonance and beyond 2.5 AU, the Hungarias, and the Phocaeas. This similarity suggests that these populations continuously

lose objects to the MCA region due to an increase in eccentricity, sustaining the MB, HU, and PH groups. Only 2% of MCAs larger than 5 km have  $a$  and  $i$  different from those non-planet-crosser asteroids and therefore must have evolved relative to the orbit they had when they first crossed the orbit of Mars: we denote them EV (Fig. 1).

To better understand the process by which non-planet-crossing asteroids become MCAs, and in particular the dynamical link between the main belt and MB populations, we have numerically integrated (7) the evolution of 412 main belt asteroids, a representative sample of the population with  $a = 2.1$  to 2.5 AU,  $i < 15^\circ$ , perihelion distance  $q < 1.8$  AU and not intersecting the orbit of Mars during the first 300,000 years. The integrations covered a time span of 100 My, along which we numerically computed the time evolution of proper elements to distinguish between regular and chaotic asteroids (8).

Integrations show that the majority of the asteroids are on chaotic orbits and 25% of them become MBs (Fig. 2). We find that this process is mainly due to mean motion resonances with Mars (3/5, 7/12, 4/7, 5/9, 7/13, and 1/2), mean motion resonances with Jupiter (7/2 and 10/3), and three-body mean motion resonances between Jupiter, Saturn, and the asteroid or Mars, Jupiter, and the asteroid (9). Although the most important source region of MBs is the one with  $a < 2.17$  AU, where high-order mean motion resonances with Mars are particularly dense, in practice, asteroids are removed from the main belt all over the 2.1- to 2.5-AU range, driven by numerous weak mean motion resonances. It is possible that a similar process also drives Hungaria and Phocaea asteroids to Mars-crossing orbits, sustaining the HU and PH populations.

To quantify the exchange of asteroids among non-planet-crossers, MCAs and ECAs, we have also integrated the evolution of 511 MCAs, a representative sample of their total population. MCAs become ECAs

F. Migliorini, Armagh Observatory, College Hill BT61 9DG, Northern Ireland, United Kingdom, and Osservatorio Astronomico di Torino, I-10025 Pino Torinese, Italy. P. Michel, Osservatorio Astronomico di Torino, I-10025 Pino Torinese, Italy, and Observatoire de la Côte d'Azur, B.P. 4229, 06304 Nice cedex 4, France. A. Morbidelli and D. Nesvorný, Observatoire de la Côte d'Azur, B.P. 4229, 06304 Nice cedex 4, France. V. Zappalà, Osservatorio Astronomico di Torino, I-10025 Pino Torinese, Italy.

\*Died on 2 November 1997 in a mountain accident. The paper is devoted to his memory.

†To whom correspondence should be addressed. E-mail: morby@obs-nice.fr